2627

NRL Report 8596

End-Fire Hybrid Array Antennas

W. K. KAHN

Airborne Radar Branch
Radar Division

July 12, 1982

NAVAL RESEARCH LABORATORY
Washington, D.C.

SECURITY CLASSIFICATION OF THIS PAGE (When Data Entered)

REPORT DOCUMENTATION PAGE		READ INSTRUCTIONS BEFORE COMPLETING FORM
1. REPORT NUMBER NRL Report 8596	2. GOVT ACCESSION NO.	3. RECIPIENT'S CATALOG NUMBER
4. TITLE (and Subtitle) END-FIRE HYBRID ARRAYS ANTENNAS		5. TYPE OF REPORT & PERIOD COVERED Interim report on a continuing NRL problem 6. PERFORMING ORG. REPORT NUMBER
7. AUTHOR(s) W. K. Kahn		8. CONTRACT OR GRANT NUMBER(s)
9. PERFORMING ORGANIZATION NAME AND ADDRESS Naval Research Laboratory Washington, DC 20375		10. PROGRAM ELEMENT, PROJECT, TASK AREA & WORK UNIT NUMBERS 62712N 53-0662-02 WF12-131-602
11. CONTROLLING OFFICE NAME AND ADDRESS Naval Air Systems Command Washington, DC 20361		12. REPORT DATE July 12, 1982 13. NUMBER OF PAGES 21
14. MONITORING AGENCY NAME & ADDRESS(if different from Controlling Office)		15. SECURITY CLASS. (of this report) UNCLASSIFIED 15a. DECLASSIFICATION/DOWNGRADING SCHEDULE

16. DISTRIBUTION STATEMENT (of this Report)

Approved for public release; distribution unlimited

17. DISTRIBUTION STATEMENT (of the abstract entered in Block 20, if different from Report)

18. SUPPLEMENTARY NOTES

19. KEY WORDS (Continue on reverse side if necessary and identify by block number)

Radar
Antenna
End-fire-arrays

20. ABSTRACT (Continue on reverse side if necessary and identify by block number)

A heuristic approach useful in the design of end-fire array antennas is described. When an array is scanned "beyond end fire," the last elements of the array, in the direction of the end-fire beam, generally receive net power transmitted by other elements of the array. This received power might conceivably be recirculated and reradiated at the price of substantial complexity in the feed network. It is relatively simple to absorb this power in appropriate resistive loads at the price of reduced gain. A compromise alternative, termination of these end elements in reactive loads especially determined to preserve desired pattern characteristics is examined.

DD FORM 1 JAN 73 1473 EDITION OF 1 NOV 65 IS OBSOLETE
S/N 0102-014-6601

SECURITY CLASSIFICATION OF THIS PAGE (When Data Entered)

CONTENTS

END-FIRE HYBRID ARRAY ANTENNAS

INTRODUCTION

This report describes a heuristic approach useful in design of end-fire hybrid-array antennas [1,2]. Hybrid arrays comprise two classes of elements: elements excited by generators either directly or through a feed network, and elements that are only excited parasitically as in the case of Yagi directors, Fig. 1. Excitation of elements in the first class can, at least in principle, be set arbitrarily. Excitation of elements in the second class is severely constrained. A simple procedure is presented for modifying an initial current distribution prescribed with certain pattern objectives in mind, to fit both hybrid array constraints and the lossless constraint. The pattern produced by the modified current distribution is then compared with that produced by the initially prescribed currents.

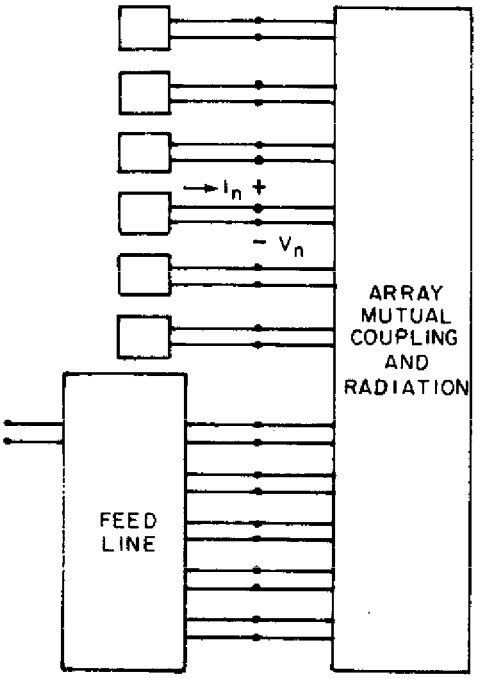

Fig. 1 — Equivalent circuit of a hybrid antenna

Current distributions for end-fire linear arrays are commonly derived as follows. A broadside pattern with the desired general characteristics is synthesized in direction cosine space. The main beam of the pattern is then scanned to end fire by means of a linear phase taper. With closely spaced arrays, a narrowing of the end-fire beam (increased directivity) may be obtained at the expense of higher relative sidelobe level by continuing to scan the main beam "beyond end fire" into the invisible region of direction cosine space [3]. We will see that such current distributions fit the hybrid array configuration rather naturally.

Manuscript submitted February 17, 1982.

When prescribed currents are impressed on the fixed mutual impedance constraint of a linear array, definite voltages appear at the antenna terminals. If these currents are phased to scan the main beam beyond end fire, voltages at several of the antennas will be found to be more than 90° out of phase with the prescribed currents. This means that these antennas *receive* power from the others and, viewed at their terminals, appear as active circuit elements. In the case of these active elements, we have the following choices. We may seek to elaborate a network that accepts the received power and feeds it back into the elements that radiate net power, or we may absorb the received power in the appropriate passive load. The second alternative, which leads to one kind of hybrid antenna, is certainly much simpler (Fig. 1). However, power lost in the loads reduces the absolute gain of the array antenna even if the directivity of the radiation patterns remains constant. We propose to modify the prescribed currents so as to eliminate this loss. The passive loads corresponding to the modified currents will then be purely reactive. Among the infinite number of possible modifications that might accomplish this, we choose one that changes the prescribed current phasor by a small (the smallest) phasor increment. The intent, of course, is also to produce only a small change in the desirable pattern characteristics. If in particular the directivity (beam width) of the pattern is substantially maintained, the elimination of loss increases the absolute gain, restoring the design value.

A network formulation of the array problem is outlined in the next section. Two ways of calculating the modified currents are given: a recursive algorithm, and a direct algebraic (matrix) solution. The recursive algorithm is advantageous for numerical computation.

A later section comprises two numerical examples. The uniform current distribution is examined as a classic example despite the fact that the associated side-lobe level may be too high for most applications. A cosine-on-pedestal distribution illustrates the low side-lobe case.

NETWORK FORMULATION

A given arrangement of antennas in space results in a definite open-circuit impedance matrix characterizing the mutual interactions of the array elements at the terminals of the antennas:

$$V_m = \sum_{n=1}^{N} Z_{mn} I_n. \tag{1}$$

These equations apply at the terminals of the array network shown on the right in Fig. 1. The positive directions for terminal voltage and current are indicated on that figure.

The complete radiation pattern of an array can be computed if the pattern radiated by any elementary antenna in the presence of all the other elements is known. When the other elements (which are not excited) are open-circuited, the element field patterns in "the open-circuited array environment," $\mathbf{f}_{l,n}^{(0)}(\theta,\phi)$, are produced by unit currents. The total radiation field pattern produced when current I_n flows into the terminal of the nth antenna, $n = 1, 2, \ldots N$, element is then found by superposition

$$\mathbf{F}(\theta,\phi) = \sum_{n=1}^{N} \mathbf{f}_{l,n}^{(0)}(\theta,\phi)\, I_n. \tag{2}$$

Since, by definition, Z_{nn} is the input impedance to the nth antenna in the open-circuited array environment, the specification of unit current excitation implies the power normalization for $\mathbf{f}_{l,n}^{(0)}(\theta,\phi)$

$$\iint_{\text{all angles}} |\mathbf{f}_{l,n}^{(0)}(\theta,\phi)|^2 \, d\Omega = \text{Re}\,\{Z_{nn}\}. \tag{3}$$

Suppose a desired pattern $\mathbf{F}(\theta,\phi)$ is obtained with some prescribed set of current, I_n.

Then, via (1), definite terminal voltages V_n appear as a response. In other words, effective input impedances

$$Z_{(n)} = \left.\frac{V_n}{I_n}\right|_{\substack{\text{all } I_m \text{ prescribed} \\ m=1,\ 2,\ \ldots,\ n,\ \ldots,\ N}} \tag{4}$$

arise at the input of each antenna. The phase of the voltage V_n relative to the current I_n determines the direction of net (average) power. A particular antenna appears

$$\text{passive if } \operatorname{Re}\{Z_{(n)}\} > 0, \tag{5a}$$

and

$$\text{active if } \operatorname{Re}\{Z_{(n)}\} < 0. \tag{5b}$$

Power from one or more coherent generators must be supplied by a feed network to all elements which appear passive. The precise character of this feed network need not be specified now. When can negative values of Re $\{Z_{(n)}\}$ be expected? They do arise in current distributions scanned "beyond end fire." Those elements, which appear active, we now choose to terminate in an appropriate passive load. These are the individual loads at the upper left-hand side of Fig. 1.

Appropriate Termination of Active Elements

As noted above, the definite mutual impedances between the given array element produces the voltage V_n at the nth port in response to *all* the prescribed currents. These values of voltage and current are consistent with only one value of impedance for the termination at an active port, Fig. 2, namely,

$$Z_{Tn} = \frac{V_n}{-I_n} = -Z_{(n)}. \tag{6}$$

For n an active port, (5b) ensures that Z_{Tn} is passive.

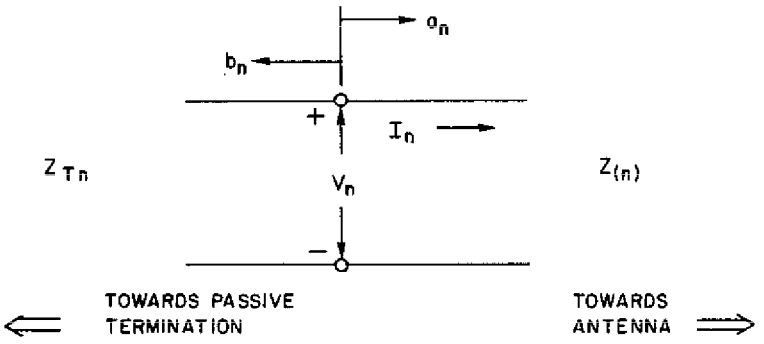

Fig. 2 — Typical array antenna port, active input impedance

Since $Z_{(n)}$ depends on the prescribed current distribution, so must the termination. Further, since the mutual coupling yielding $Z_{(n)}$ depends on frequency in some definite way, even the frequency dependence of Z_{Tn} must, in principle, follow. A different termination Z_{Tn}^{a} may be selected in place of Z_{Tn} only at the price of some deviation in the I_n, and consequently in the radiation pattern, from the prescribed values.

Reactive Terminations, Z_{Tn}^{q}

Compared to the terminations Z_{Tn} required at the active antenna ports for the prescribed currents, reactive terminations Z_{Tn}^{q} offer two advantages: one set of losses is eliminated from the array antenna, and the reactive terminations are easily realized in low loss transmission line leads. An algorithm leading to particular reactances and the corresponding perturbed currents is presented next.

The voltages V_n and currents I_n at the antenna terminals can be expressed in terms of wave amplitudes a_n incident onto the antenna and b_n reflected from the antenna

$$2\sqrt{R_{an}}\, a_n = V_n + R_{an} I_n \tag{7a}$$

$$2\sqrt{R_{an}}\, b_n = V_n - R_{an} I_n \tag{7b}$$

where R_{an} are normalization numbers. It will be convenient to take R_{an} equal to the characteristic impedance of the transmission line attached to the nth element. Each antenna element is assumed to have been tuned or matched to this characteristic impedance with all other antenna elements open-circuited.

Physically then, the waves b_n are produced by mutual coupling from the other antenna elements, especially those elements strongly excited by the feed network. To first order, this wave is treated as a constant. The wave a_n is regarded as due to reflection from the termination. The algorithm modifies this reflected wave. We take the incident and reflected waves that obtain with the prescribed currents as zero order initial values in our algorithm and denote them $I_n^{(0)}$, $a_n^{(0)}$, $b_n^{(0)}$, etc. The composition of wave phasors a and b into the current phasor I,

$$\sqrt{R_k}\, I = a - b \tag{7c}$$

is shown in Fig. 3a (solid vectors). Superscripts and subscripts have been dropped since the same construction can be applied at any stage of the algorithm and at any port. The proposed modified value of a is shown dashed. The modified value of a is obtained by adding the smallest (magnitude) increment Δa that produces a resultant with the same magnitude as b. Clearly the smallest such increment Δa must be in phase with a; we may say the modification keeps the angle of the reflection coefficient b/a constant. For fixed b, Δa is directly proportional to a change in I, ΔI. The smallest Δa therefore corresponds to the smallest ΔI. The argument is approximate since, actually, b_n does depend on all the a_m, $m = 1, \ldots, N$. In order not to confuse the diagram the modified value of the difference (7c) is not drawn in. The particular choice of Δa is clarified by phasor diagrams illustrating two alternative possibilities: magnitude of I constant (Fig. 3b), and phase of I constant (Fig. 3c). These alternatives were not studied in detail.

From any given set of incident and reflected waves we compute a modified set as follows:

$$\left.\begin{aligned} a_n^{(s)'} &= a^{(s)} \\ b_n^{(s)'} &= b^{(s)} \end{aligned}\right\} \quad \text{passive ports,} \tag{8a}$$

$$\left.\begin{aligned} a^{(s)'} &= |\Gamma_{(n)}^{(s)}|\, a^{(s)} \\ b^{(s)'} &= b^{(s)} \end{aligned}\right\} \quad \text{active ports,} \tag{8b}$$

where the effective reflection coefficient

$$\Gamma_{(n)}^{(s)} = \frac{b_n^{(s)}}{a_n^{(s)}}. \tag{9}$$

The modified set of waves leads to new currents (at the active ports)

$$\sqrt{R_{gn}}\, I_n^{(s+1)} = a_n^{(s)'} - b_n^{(s)'}. \tag{10}$$

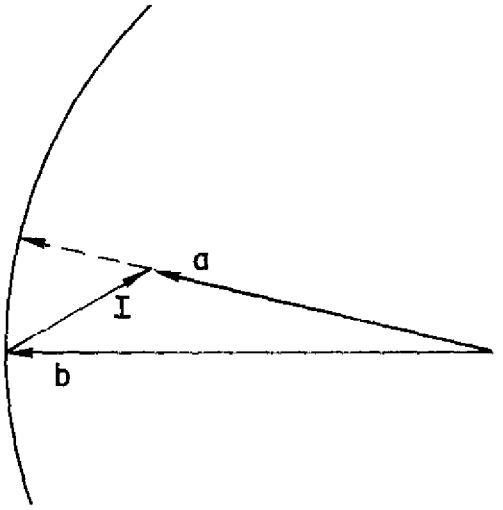

(a) Minimum increment ΔI, constant angle of reflection coefficient

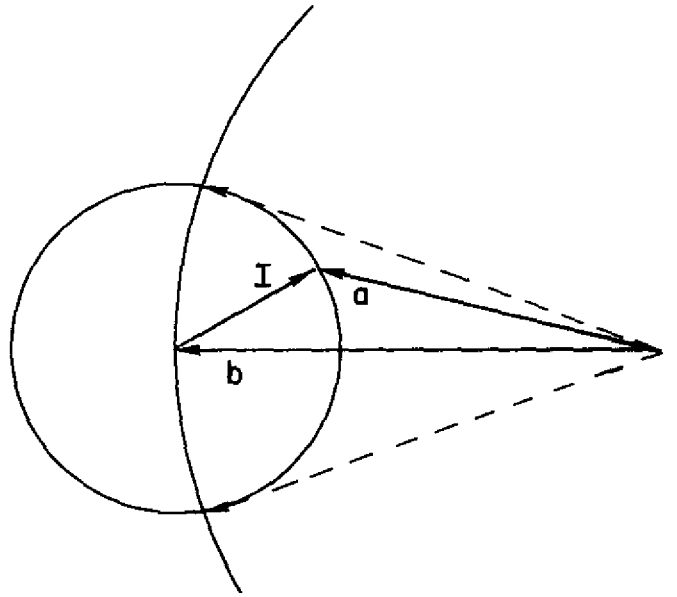

(b) Constant magnitude of current, $|I|$ = constant

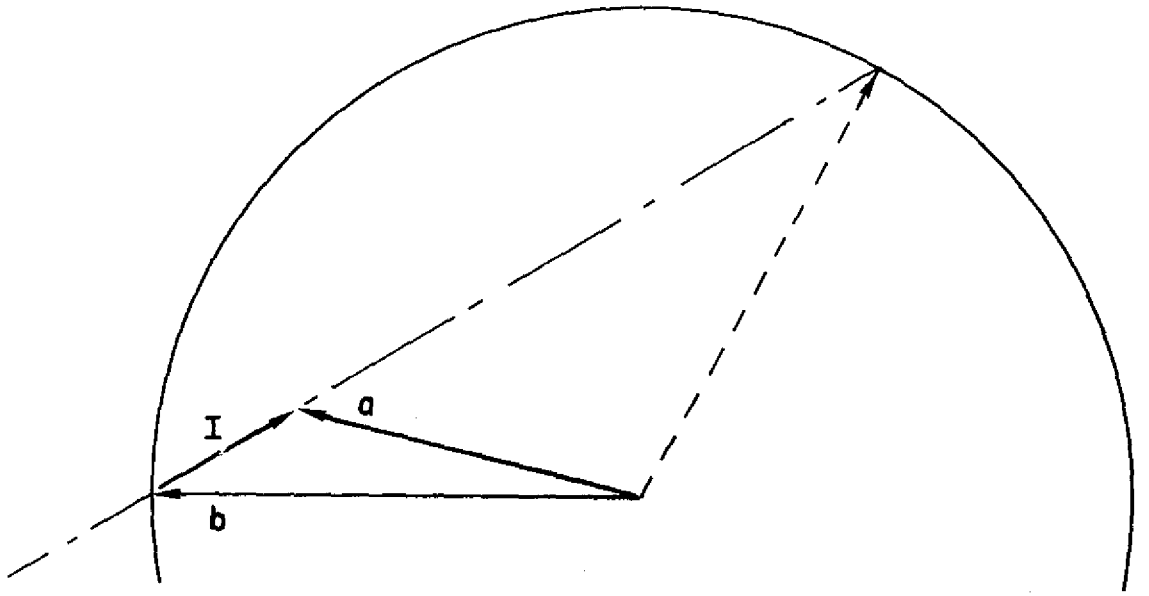

(c) Constant phase of current, $\angle I$ = constant

Fig. 3 — Composition of wave phasors a and b into the current phasor I

These new currents lead to an entirely new set of voltages $V_n^{(S+1)}$ via (2). The new voltages and currents define new incident and reflected waves $a^{(S+1)}$ and $b^{(s+1)}$ via (7). Starting with the prescribed currents $s = 0$ the process may be repeated until $|\Gamma_{(n)}^{(s)}|$ is sufficiently close to unity for all active ports. Occasionally the new current distribution may have the effect of turning a previously passive antenna element into an active one. In the examples studied, this algorithm was found to converge rapidly.

The constraint of maintaining the angle of the reflection coefficient may also be used in a direct calculation of the modified currents. We rewrite (2) in matrix form:

$$\underline{V} = \begin{pmatrix} \underline{V}_\alpha \\ \hline \underline{V}_\beta \end{pmatrix} = \left(\begin{array}{c|c} Z_{\alpha\alpha} & Z_{\alpha\beta} \\ \hline Z_{\beta\alpha} & Z_{\beta\beta} \end{array}\right) \begin{pmatrix} \underline{I}_\alpha \\ \hline \underline{I}_\beta \end{pmatrix} = Z\underline{I}, \tag{11}$$

where the matrices are partitioned to separate out quantities relating passive elements α and quantities relating to active elements β. Inserting the prescribed currents $\underline{I}^{(0)}$, we find the voltages $\underline{V}^{(0)}$ and the reflection coefficients $\Gamma_n^{(0)}$ as before. The *angles* of these reflection coefficients are used to compute reactive loads,

$$Z_{(n)}^{(h)} = \frac{|\Gamma_{(n)}^{(0)}| + \Gamma_n^{(0)}}{|\Gamma_n^{(0)}| - \Gamma_n^{(0)}}, \tag{12}$$

for all active elements in the hybrid antenna. These reactances are ordered into a diagonal square matrix,

$$Z_{\beta\beta}^{(h)} = \text{diag}\,\{Z_{(n)}^{(h)}\}. \tag{13}$$

Now

$$Z_{\beta\beta}^{(h)}\,\underline{I}_\beta^{(h)} = Z_{\beta\alpha}\underline{I}_\alpha^{(0)} + Z_{\beta\beta}\underline{I}_\beta^{(h)}, \tag{14}$$

where $\underline{I}_\beta^{(h)}$ are the desired modified currents at the active element ports. Solving for

$$\underline{I}_\beta^{(h)} = \left(Z_{\beta\beta}^{(h)} - Z_{\beta\beta}\right)^{-1} Z_{\beta\alpha}\underline{I}_\alpha^{(0)}. \tag{15}$$

Although this formulation is attractive algebraically, problems of computational accuracy arise.

Transmission Loss, Efficiency

The efficiency factor to be evaluated here accounts for the power dissipated in the terminations Z_{Tn}. In the first instance, it represents the price paid for reducing size and complexity of the feed network so that it connects only to the passive array elements. It translates directly into decreased absolute antenna gain.

To obtain an upper bound efficiency, we assume that the feed network has no internal dissipation and that reflection losses at the input to the feed network have been eliminated by proper design. Therefore, the input power is the power absorbed by the passive array elements:

$$P_{IN} = \sum_{\substack{\text{passive} \\ \text{ports}}} |I_n|^2 \,\text{Re}\, Z_{(n)} = \sum_{\substack{\text{passive} \\ \text{ports}}} \{|a_n|^2 - |b_n|^2\}. \tag{16}$$

The power lost in the terminations attached to the active elements is

$$P_{TL} = \sum_{\substack{\text{active} \\ \text{ports}}} |I_n|^2 \,\text{Re}\, Z_{Tn} = \sum_{\substack{\text{active} \\ \text{ports}}} \{|b_n|^2 - |a_n|^2\}. \tag{17}$$

The efficiency factor, accounting for this loss in power actually radiated, P_{RAD}, is

$$\eta = \frac{P_{RAD}}{P_{IN}} = 1 - \frac{P_{TL}}{P_{IN}}. \tag{18}$$

It is convenient to express this efficiency as an equivalent transmission coefficient in decibels,

$$\text{dB } T = 10 \log_{10} \eta. \tag{19}$$

Remark on Peak Power Capacity of the Feed Network

For a given array, the input impedances $Z_{(n)}$ corresponding to prescribed currents I_n are fixed. Consequently, relative to a given source impedance level R_{gn}, one has incident and reflected wave amplitudes (7). The effective reflection coefficients, $\Gamma_{(n)}$, must have magnitudes less than unity for the elements connected to the feed network, but for the current distributions of interest here these magnitudes do intrinsically approach unity. Tuning transmission line transformers are conventionally employed. Typically, field intensities within such resonant tuning structures are enhanced above the input levels in proportion to the square root of the VSWR matched out. This incidental feature may be an important limiting feature in design.

NUMERICAL RESULTS: A PLANAR ARRAY OF LINE SOURCES

To demonstrate the utility of the algorithm developed in the preceding section for realization of a lossless hybrid antenna design, the theory is now applied to an array of equally spaced line sources. This configuration was selected because of its simplicity and because it models an array of interest in connection with a specific airborne radar application. Two sets of prescribed initial current distributions are considered: a uniform distribution and a cosine-on-pedestal distribution.

Consider the array of N line sources shown in Fig. 4. The line currents extend indefinitely in the X direction. The elements are uniformly spaced along the y axis, D wavelengths apart. Adapted to this two-dimensional case, Eq. (1) for the radiation field becomes,

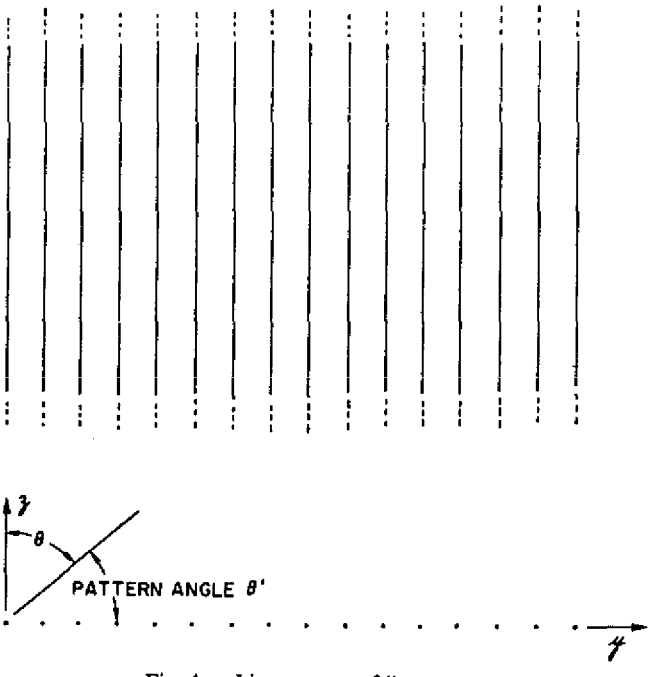

Fig. 4 — Linear array of line sources

$$F(\theta) = \sum_{n=1}^{N} \mathbf{f}_{i,n}^{(0)}(\theta)\, I_n. \tag{20}$$

For idealized line sources the element patterns in the open-circuited array environment are all identical and isotropic. Consequently,

$$\sqrt{2\pi} F(\theta) = \sum_{n=1}^{N} I_n\, e^{j2\pi(n-1)D\sin\theta}, \tag{21}$$

where the exponential factor accounts for the relative location of the elements. The elements of the open circuit impedance matrix are known [4,5]

$$Z_{mn} = 1, \quad m = n, \tag{21a}$$

$$Z_{mn} = H_0^{(2)}(2\pi D|m-n|), \quad m \neq n; \tag{22b}$$

where $H_0^{(2)}$ is the zeroth order Hankel function of the second kind.

A classic distribution consists of currents with uniform amplitude and linearly progressive phase:

$$I_n = \epsilon^{-j\beta(n-1)}. \tag{23}$$

The peak of the resulting radiation pattern, corresponding to in-phase addition of radiation from each element, occurs at values of θ such that

$$2\pi D\sin\theta - \beta = 2\pi\nu \tag{24}$$

where ν is any integer. This is located at end fire, say $\theta = -\frac{\pi}{2}$, when $\beta = -2\pi D$. All the values of $\sin\theta$ for in-phase addition are in Fig. 5a. This particular figure has been drawn using $D = 0.333$. For values of D less than one-half wavelength, $D < 0.5$, there is a range of β for which the in-phase addition peak is placed in the invisible region,

$$1 < \left|\frac{\beta}{2\pi D}\right| < \frac{1}{D} - 1. \tag{25}$$

When β is in this range, the actual beam is narrowed to the portion left in visible space, $-1 < \sin\theta < +1$, and the relative side-lobe level appears correspondingly raised (Fig. 5b).

An alternative way of stating the same condition (in terms of the total phase shift across the antenna aperture) is conventional for surface wave antennas,

$$\Phi = [\beta - 2\pi D](N-1), \tag{26}$$

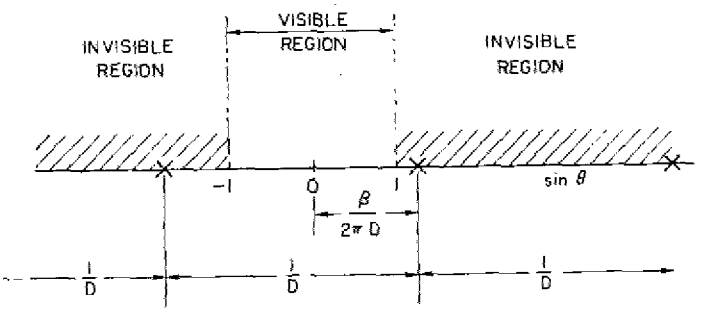

Fig. 5a — Location of in-phase addition peaks in sin θ space, marked X

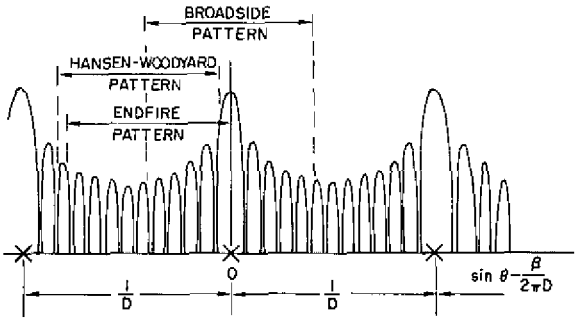

Fig. 5b — Relationship of broadside end fire and Hansen-Woodyard patterns

where Φ is the excess phase shift of the surface wave over the aperture compared to the phase shift that would be experienced by a plane wave traversing the same aperture. The Hansen-Woodyard condition for enhanced end-fire gain corresponds to an excess phase Φ of 180° [3].

For an array of 16-line currents ($N = 16$), spaced one-third wavelength apart ($D = 0.333$), direct computation shows that all antenna elements remain passive for values of Φ less than about 150°. For $\Phi = 200°$, the first 10 elements are passive and the remaining six appear active. Specifically, the input reflection coefficients $\Gamma_{(n)}$ at the inputs to the 16 antenna elements are listed in the upper part of Table 1 together with the prescribed uniform current distribution which gave rise to them. The perturbed distribution obtained by applying our algorithm is listed in the lower part of the table. It will be seen that elements 11 through 16 now have reflection coefficients of magnitude unity. These elements are passive and can be terminated in reactances Z_{Tn}. The corresponding power patterns are shown in Fig. 6. The solid curve corresponds to the prescribed currents while the broken curve is obtained using the new currents. The half-power beamwidth is not substantially changed while the side-lobe level has increased from the original value of −7.4 dB to −6.8 dB. Assuming the active elements terminated in passive loads, the original distribution is associated with an efficiency (loss factor) of −0.83 dB. This loss is eliminated by the hybrid distribution. Assuming no change in antenna directivity (possibly a somewhat optimistic estimate in view of the high side-lobe level present in this case) the antenna gain would be enhanced by the same +0.83 dB.

The second distribution to be considered consists of currents with symmetrically tapered amplitudes and linearly progressive phase:

$$I_n = \left[0.55 - 0.45 \cos \frac{2\pi}{(N-1)}(n-1)\right] \epsilon^{-j\beta(n-1)}, \tag{27}$$

a cosine-on-pedestal distribution. The peak of the resulting pattern corresponding to in-phase addition of radiation from each element is positioned by the choice of β. As discussed previously, the end-fire beam may be narrowed through an excess progressive phase shift across the aperture.

For an array of 16-line currents ($N = 16$) spaced one-third wavelength apart ($D = 0.333$), direct computation shows that for $\Phi = 350°$, the first 10 elements remain passive while the remaining six elements appear active. Specifically, the input reflection coefficients $\Gamma_{(n)}$ at the inputs to the 16 antenna elements are listed in the upper part of Table 2 together with the prescribed cosine-on-pedestal current distribution. In the lower part of the table we list the modified distribution obtained by applying an algorithm Eqs. (8), (9), and (10). Elements 11 through 16 finally have reflection coefficients of magnitude unity. Power patterns are shown in Fig. 7a. The solid curve corresponds to the prescribed

Table 1 — End-Fire Array of Line Sources

Prescribed Current Distribution: Uniform				
Currents, I_n			Reflection Coefficients, $\Gamma_{(n)}$	
Absolute, dB	Degrees	n	Absolute	Degrees
0.0000000	0.0000000	1	.3173607	−179.2471000
0.0000000	−133.2133500	2	.2786949	84.1681520
0.0000000	93.5733340	3	.3534521	65.9763950
0.0000000	−39.6399460	4	.5003036	64.5227510
0.0000000	−172.8533300	5	.6198492	54.3912660
0.0000000	53.9333950	6	.6420614	51.2610020
0.0000000	−79.2798770	7	.7265171	54.4738080
0.0000000	147.5067400	8	.8360424	50.2193220
0.0000000	14.2933390	9	.8401902	48.2400820
0.0000000	−118.9198300	10	.8989694	52.8832550
0.0000000	107.8667800	11	1.0365400	50.6579440
0.0000000	−25.3463820	12	1.0244148	48.1973190
0.0000000	−158.5597500	13	1.0466812	55.0822910
0.0000000	68.2268520	14	1.2812850	55.3434370
0.0000000	−64.9865420	15	1.2326851	49.3651810
0.0000000	161.8000800	16	1.0716577	61.0628810
Modified Current Distribution				
−.9627366	0.0000000	1	.3425306	177.5227100
−.9627376	−133.2133500	2	.2823270	80.4581450
−.9627376	93.5733340	3	.3372738	65.8717350
−.9627366	−39.6399460	4	.5099453	66.1048890
−.9627366	−172.8533300	5	.6274173	53.3010030
−.9627366	53.9333950	6	.6286440	50.9195560
−.9627343	−79.2798770	7	.7321156	55.7640150
−.9627366	147.5067400	8	.8470640	49.3398280
−.9627366	14.2933390	9	.8238122	47.7418210
−.9627376	−118.9198300	10	.9027936	54.6525270
−.7521589	111.1185900	11	1.0004737	50.1802370
−.9035276	−24.4328160	12	1.0018158	47.0877150
−.7485329	−155.9007900	13	.9978949	57.5681000
0.0000000	83.7651520	14	1.0040879	58.0629810
−.0840324	−48.4991150	15	1.0059035	47.0680770
−.2709647	170.5925000	16	1.0082133	55.3905940

Element Spacing, $D = 0.333$
Excess Phase Across Aperture, $\Phi = 200°$

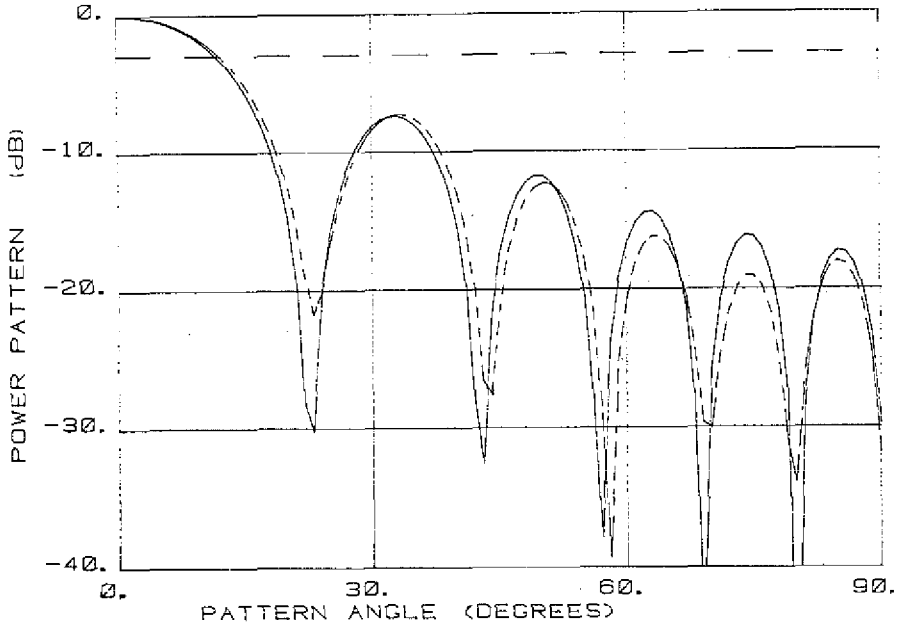

Fig. 6 — Power pattern—uniform distribution; excess phase delay aperture = 200°, D = 0.333

currents, and the broken curve to the new perturbed currents. The half-power beamwidth is not substantially changed but the side-lobe level has increased from −29.6 to −22.5 dB. Assuming the active elements terminated in the required passive loads, the original distribution is associated with an efficiency (transmission loss factor) of −1.69 dB. This loss is eliminated by the final hybrid current distribution and the associated reactive loads. In view of the low side-lobe level, the 3 dB beamwidth is a good measure of directivity. The directivity of the perturbed pattern is seen to be the same as that of the original. The antenna gain would therefore be enhanced by 1.69 dB through elimination of loss in the passive terminations.

Figures 7b-7g display patterns obtained with the same configuration $N = 16$, $D = 0.333$, for various values of excess phase: $\Phi = 250°$, 275°, 300°, 325°, 375°, and 400°. The expected trends, narrowing of the main beam accompanied by a rising side-lobe level, are evident. The efficiencies accompanying the prescribed distributions are listed in Table 3.

Finally, the value of the perturbed illumination would be curtailed if the reactive terminations required by the perturbed illumination was highly frequency sensitive. In fact, mutual coupling effects do not lead to a rapid change with frequency. The dependence of the phase of the required load reflection coefficient for the cosine-on-pedestal distribution as a function of the element spacing in fractional wavelengths is listed in Table 4. Both the nominal values and the final values arising from the algorithm used to compute the hybrid currents are given. The excess phase is kept constant, $\Phi = 350°$. The patterns corresponding to $D = 0.300$ and $D = 0.366$ are shown in Figs. 8a and 8b.

Table 2 — End-Fire Array of Line Sources

Prescribed Current Distribution Cosine on Pedestal				
Currents, I_n			Reflection Coefficients, $\Gamma_{(n)}$	
Absolute, dB	Degrees	n	Absolute	Degrees
−20.0000040	0.0000000	1	.2130976	−175.9291700
−17.1456720	−143.2133500	2	.3077611	145.8230900
−12.0798070	73.5733490	3	.4269505	131.2961400
−7.7243834	−69.6399990	4	.4392397	115.8314100
−4.4799671	147.1467000	5	.4551377	105.4489400
−2.2139678	3.9333482	6	.5140839	97.1759640
−.7805297	−139.2799700	7	.5966804	88.3632510
−.0858371	77.5068050	8	.6772606	80.7492520
−.0858371	−65.7066500	9	.7754637	75.3220830
−.7805274	151.0801400	10	.9186242	69.6708830
−2.2139626	7.8667021	11	1.0925035	61.8186260
−4.4799623	−135.3467400	12	1.2913463	52.5559230
−7.7243738	81.4400330	13	1.5524104	38.8574370
−12.0798070	−61.7731930	14	1.6235037	17.7278290
−17.1456640	155.0136100	15	1.4347713	3.1590972
−20.0000040	11.7999420	16	1.3389120	−6.6487675
Modified Current Distribution				
−19.9141650	0.0000000	1	.2425795	−178.2760300
−17.0598340	−143.2133500	2	.3057822	141.2815900
−11.9939710	73.5733490	3	.4118199	131.7644000
−7.6385489	−69.6399990	4	.4417697	116.9598100
−4.3941307	147.1467000	5	.4607187	105.1646900
−2.1281309	3.9333482	6	.5122470	96.7350920
−.6946931	−139.2799700	7	.5939797	88.6706850
0.0000000	77.5068050	8	.6811055	80.8653720
0.0000000	−65.7066500	9	.7746645	74.9734040
−.6946907	151.0801400	10	.9143010	70.0936130
−1.7412503	12.3237780	11	1.0000257	64.1865080
−3.5608387	−119.9822800	12	1.0138125	54.6581730
−7.2102127	115.2657900	13	1.0087774	37.9970700
−15.3026290	−1.8972154	14	1.0037103	15.6154560
−31.9987640	−116.9347800	15	1.0005631	2.5485959
−27.3259320	−56.3557210	16	.9890641	−4.7701597

Element Spacing, $D = 0.333$
Excess Phase Across Aperture, $\Phi = 350°$

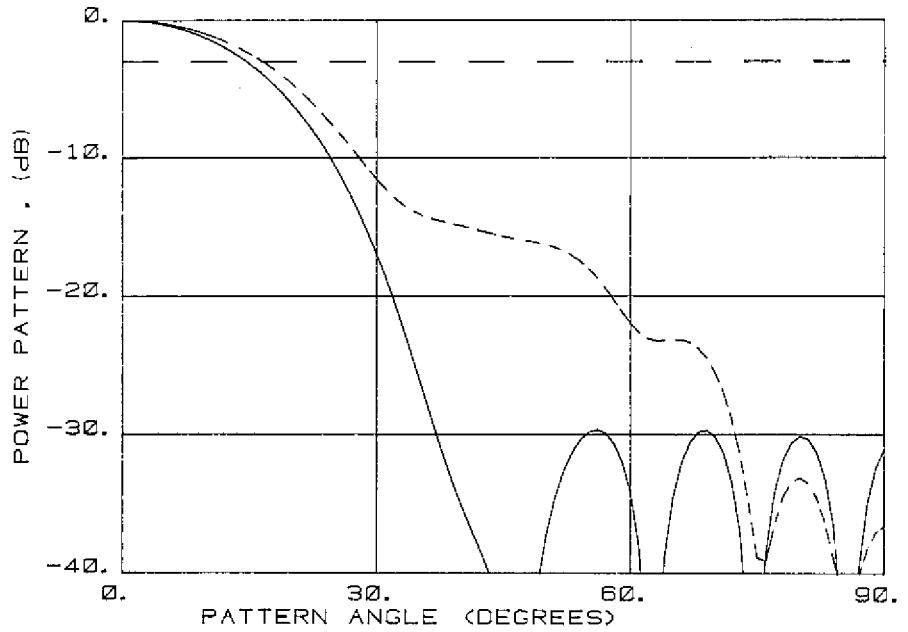

Fig. 7a — Power pattern—cosine on pedestal: prescribed current ——, reactive loads ———, excess phase delay aperture = 350°, D = 0.333 wavelength

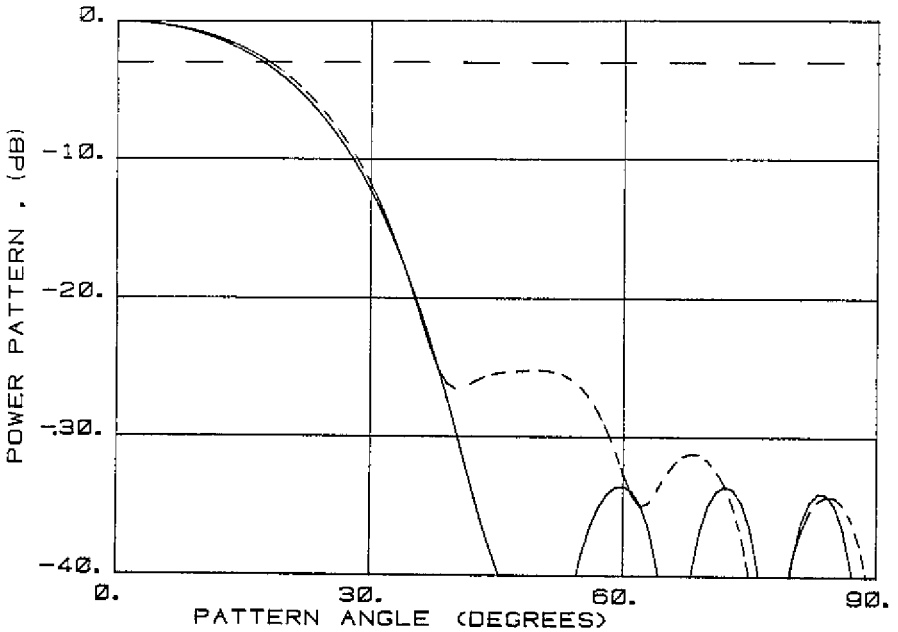

Fig. 7b — Power pattern—cosine on pedestal: prescribed current ——, reactive loads ———, excess phase delay aperture = 250°, D = 0.333 wavelength

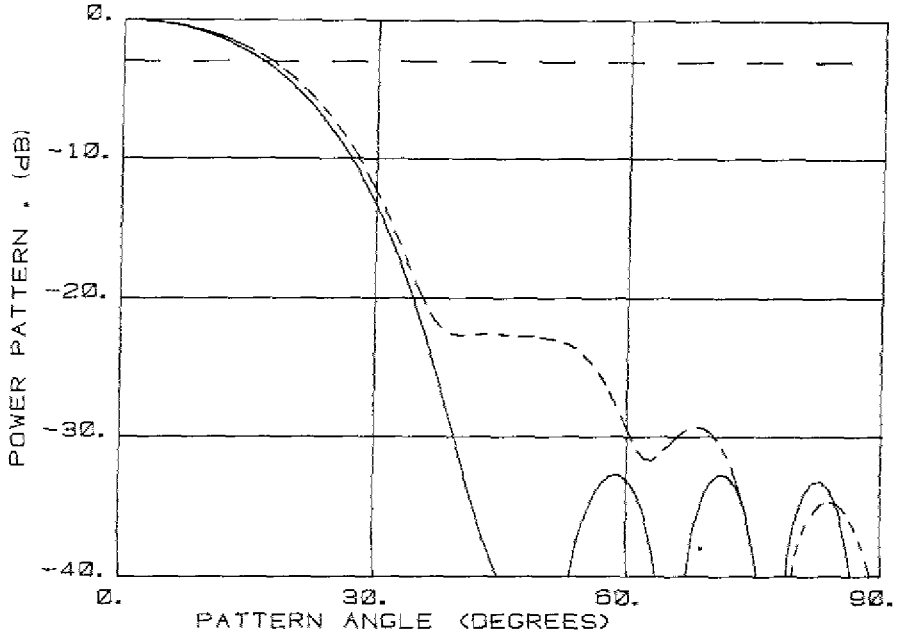

Fig. 7c — Power pattern—cosine on pedestal: prescribed current ——, reactive loads – – – – –, excess phase delay aperture = 275°, D = 0.333 wavelength

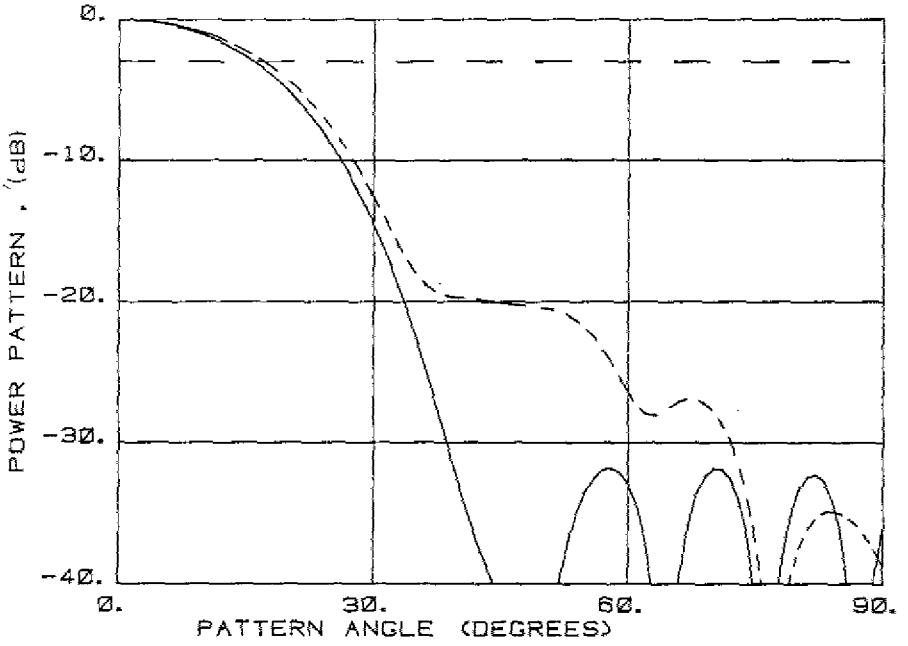

Fig. 7d — Power pattern—cosine on pedestal: prescribed current ——, reactive loads – – – – –, excess phase delay aperture = 300°, D = 0.333 wavelength

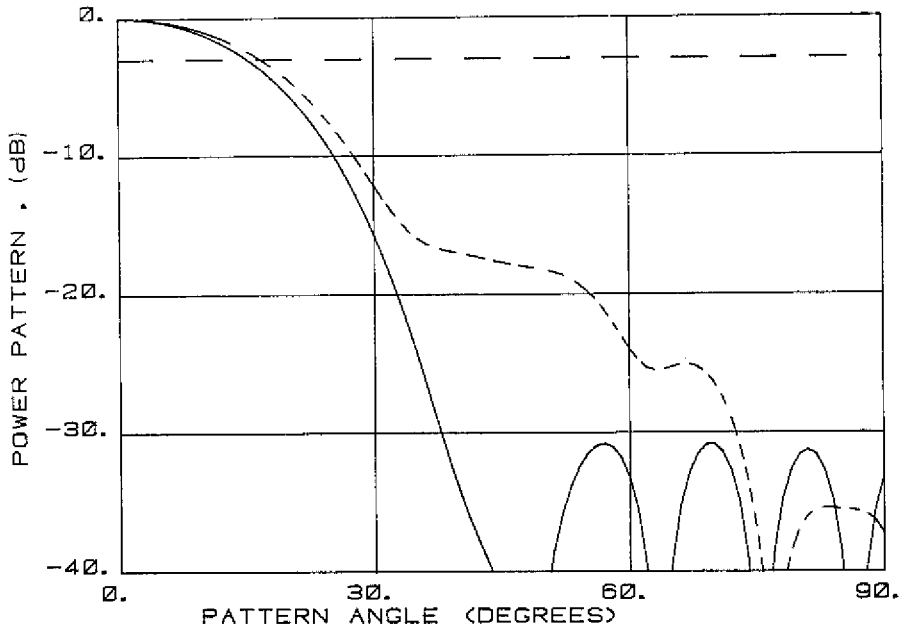

Fig. 7e — Power pattern—cosine on pedestal: prescribed current ——, reactive loads – – – – –, excess phase delay aperture = 325°, D = 0.333 wavelength

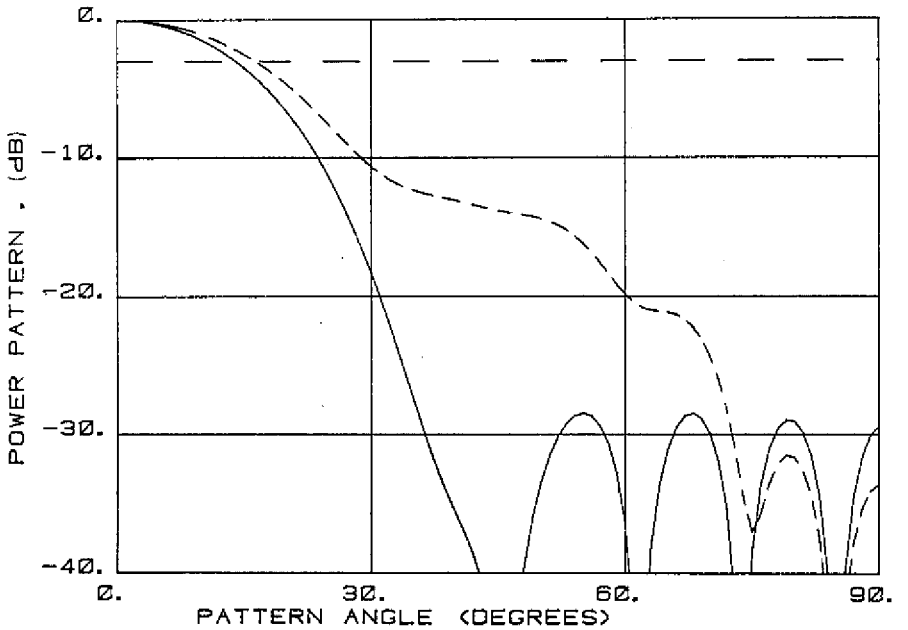

Fig. 7f — Power pattern—cosine on pedestal: prescribed current ——, reactive loads – – – – –, excess phase delay aperture = 375°, D = 0.333 wavelength

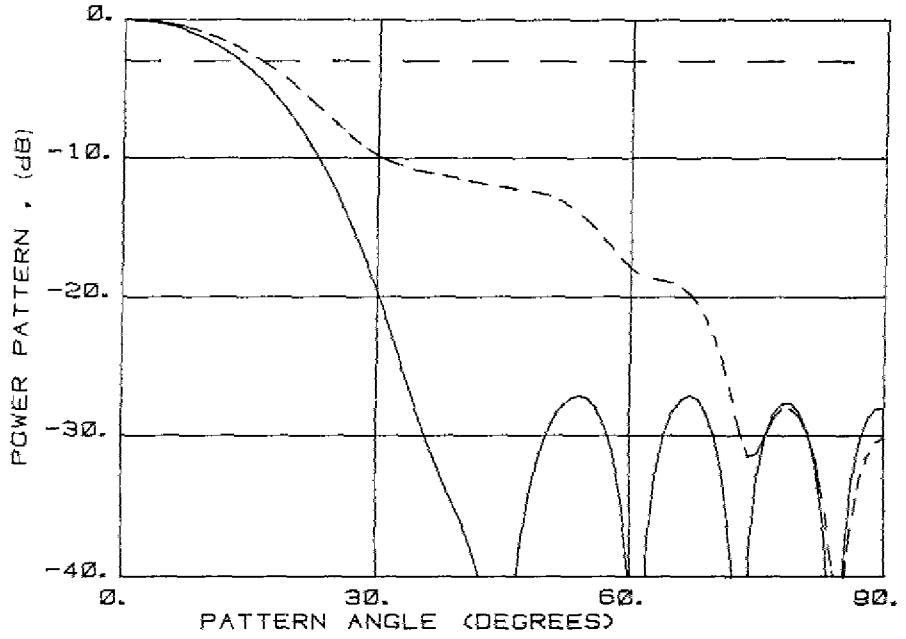

Fig. 7g — Power pattern—cosine on pedestal: prescribed current ——, reactive loads – – – –, excess phase delay aperture = 400°, D = 0.333 wavelength

Table 3 — Efficiencies
at Prescribed Distributions

Excess phase, Φ (deg)	Efficiency (dB)
200	−0.3
250	−0.7
275	−0.9
300	−1.2
325	−1.4
350	−1.7
375	−1.9
400	−2.1

Table 4 — Angle of the Active Reflection Coefficient, Angle $\{\Gamma_{(n)}\}$

Element	Element Spacing					
	D = 0.300		D = 0.333		D = 0.366	
n	initial (deg)	final (deg)	initial (deg)	final (deg)	initial (deg)	final (deg)
11	63.5	66.3	61.8	64.2	60.2	62.6
12	51.6	53.1	52.6	54.7	53.0	55.0
13	36.8	36.0	38.9	38.0	39.8	39.1
14	16.3	14.1	17.7	15.6	20.0	17.9
15	2.3	1.8	3.2	2.5	4.0	3.2
16	−6.2	−5.9	−6.6	−4.8	−7.1	−6.3

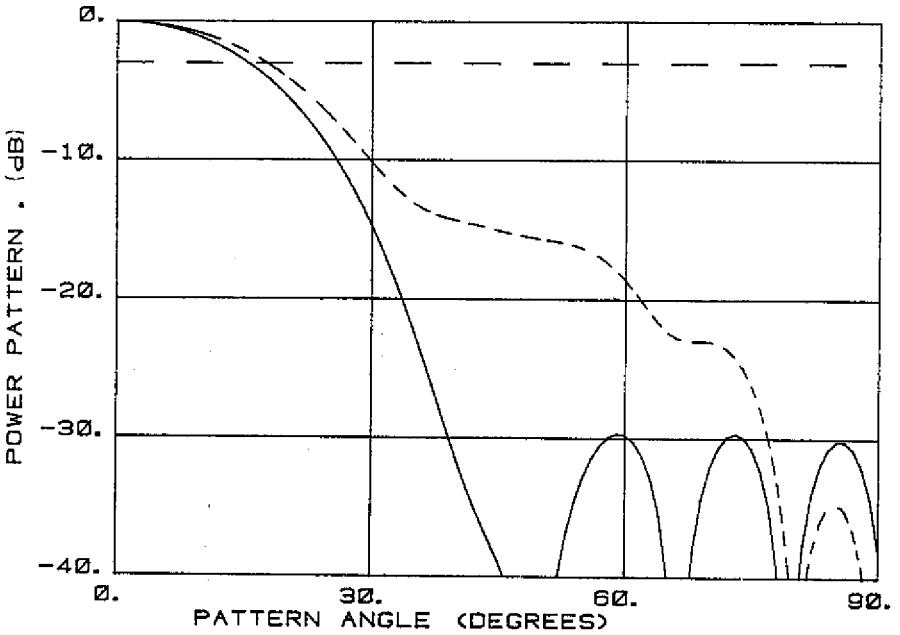

Fig. 8a — Power pattern—cosine on pedestal: prescribed current ——, reactive loads – – – – –, excess phase delay aperture = 350°, D = 0.300 wavelength

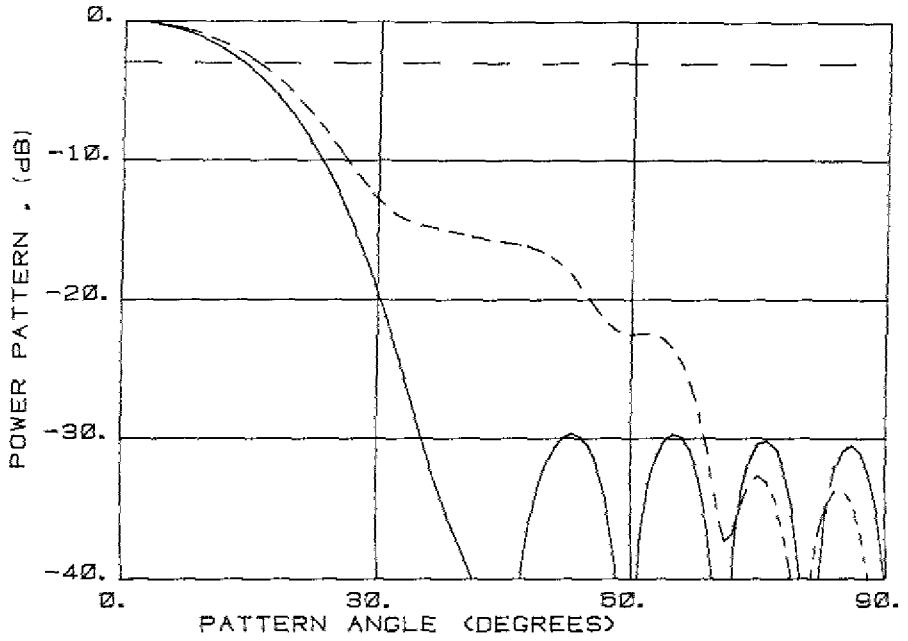

Fig. 8b — Power pattern—cosine on pedestal: prescribed current ——, reactive loads – – – – –, excess phase delay aperture = 350°, D = 0.366 wavelength

Table 5 — Comparative Pattern Characteristics

Prescribed Cosine-on-Pedestal				Modified Illumination		
Excess Phase (deg)	Directivity (dB)	Loss (dB)	Gain (dB)	Gain (dB)	Δ Gain (dB)	Side-lobe* (dB)
250	10.2	−0.8	9.4	10.0	0.6	−25.2
275	10.4	−0.9	9.5	10.1	0.6	−22.6
300	10.5	−1.2	9.3	10.2	0.9	−20.0
325	10.8	−1.4	9.4	10.3	0.9	−17.8
350	11.0	−1.7	9.0	10.5	1.5	−15.5
375	11.1	−1.9	9.2	10.5	1.3	−13.0
400	11.2	−2.1	9.1	10.5	1.4	−11.4

*Cosine-on-pedestal side-lobe level < 25 dB

CONCLUSIONS

When an array antenna is scanned "beyond end fire" to achieve a degree of superdirective narrowing of the pattern, the direction of power in some of the antenna elements may reverse. In particular, the last elements of the array in the direction of the end-fire beam tend to receive power transmitted by the other elements of the array. This received power might conceivably be recirculated, but is more conveniently absorbed in loads. The resulting loss must then be charged against the enhanced directivity in computing gain. The alternative studied in this report, a modification of the illumination which reduces the absorbed power to zero (reactive termination), preserves desired pattern characteristics to the extent shown in the power patterns of Figs. 7 and 8 and summarized in Table 5.

Although the directivity is enhanced by about 1 dB when the beam is scanned beyond end fire, the enhanced directivity is accompanied by a slight loss in gain. The loss in gain may be offset by modifying the current distribution as discussed in the report. The optimum in terms of gain is then very broad. The rapid deterioration in the side-lobe level indicates that scan "beyond end fire" technique is subject to rapidly diminishing returns. More sophisticated modifications of the initial current distribution may soften this last conclusion.

ACKNOWLEDGMENT

The author is grateful to Dr. T. L. ap Rhys for his interest and valuable comments.

REFERENCES

1. W.K. Kahn, "Center-Fed Leaky-Wave Yagi Hybrid Antenna," Navy Tech. Disclosure Bulletin, **3**; 8, August 1978, pp. 60-62.

2. W.K. Kahn, "Double-Ended Backward-Wave Yagi Hybrid Antenna," IEEE Transactions on Antennas and Propagation, **AP-29**; 3, May 1981, pp. 530-532.

3. R.S. Elliott in R.C. Hansen (Editor), *Microwave Scanning Antenna*, **II**, Ch. I, Academic Press, 1966.

4. W. Wasylkiwskyj and W.K. Kahn, "Coupling, Radiation and Scattering by Antennas," Proceedings of the Symposium on Generalized Networks, April 12, 13, 14, 1966; Microwave Research Institute Symposia Series, **16**; 83-14, Polytechnic Press of the Polytechnic Institute of Brooklyn, 1966.

5. W. Wasylkiwskyj and W.K. Kahn, "Theory of Mutual Coupling Among Minimum Scattering Antennas," IEEE Transactions on Antennas and Propagation, **AP-18**, March 1970, pp. 204-216.